Chemical Geology 343 (2013) 99–110

Contents lists available at SciVerse ScienceDirect

Chemical Geology

journal homepage: www.elsevier.com/locate/chemgeo

Can biological toxicity drive the contrasting behavior of platinum and gold in surface environments?

Joël Brugger [a,b,*], Barbara Etschmann [a], Cornelia Grosse [c], Colin Plumridge [d], John Kaminski [d], David Paterson [e], Sahar Saad Shar [f], Christine Ta [g], Daryl L. Howard [e], Martin D. de Jonge [e], Andrew S. Ball [h], Frank Reith [a,i,*]

[a] School of Earth and Environmental Sciences, Centre of Tectonics, Resources and Exploration (TRaX), The University of Adelaide, North Terrace, SA 5005, Australia
[b] South Australian Museum, Department of Mineralogy, Adelaide, SA 5000, Australia
[c] Martin Luther University Halle-Wittenberg, Institut für Biologie/Mikrobiologie, DE-06120 Halle, Germany
[d] Rimfire Pacific Mining NL Suite 411, 530 Little Collins Street Melbourne, VIC 3000, Australia
[e] Australian Synchrotron, 800 Blackburn Road, Clayton, VIC 3168, Australia
[f] School of Biological Sciences, Faculty of Science and Engineering, Flinders University, Adelaide, SA 5001, Australia
[g] School of Chemical and Physical Sciences, Faculty of Science and Engineering, Flinders University, Adelaide, SA 5001, Australia
[h] School of Applied Sciences, RMIT University, PO Box 71, Bundoora, VIC 3083, Australia
[i] CSIRO Land and Water, Environmental Biogeochemistry, PMB2, Glen Osmond, SA 5064, Australia

ARTICLE INFO

Article history:
Received 30 August 2012
Received in revised form 11 February 2013
Accepted 11 February 2013
Available online 18 February 2013

Editor: J. Fein

Keywords:
Gold
Platinum
Microbiology
Environmental mobility of precious metals
Synchrotron radiation
Fifield New South Wales, Australia

ABSTRACT

In spite of the similar chemical properties of gold (Au) and platinum (Pt), Au is highly mobile in surface environments, whereas Pt appears to be far less so. In this study we assess if geomicrobial processes are likely to cause these differences, as the mobility of Pt and Au should differ little based on thermodynamic solubility alone. To achieve an accurate comparison it is important that both metals occur in the same environment. Mineral- and groundwater samples were obtained from the Fifield Pt–Au field in New South Wales, Australia, where Pt and Au nuggets occur in a series of Tertiary eluvial and alluvial paleo-placers. In particular, we studied the μm-scale dispersion of Au and Pt within an extraordinary 10 mm-sized fragment of ferruginous paleochannel material, which contained abundant native Au- and isoferroplatinum grains. Gold grains displayed complex secondary morphologies indicative of biogeochemical transformations, whereas isoferroplatinum grains appeared smooth and well-rounded and showed no signs of supergene transformation. Gold grains were surrounded by a dusting of highly pure metallic Au particles (<10 nm to >10 μm in diameter), whereas no metallic Pt particles were detected. A search for ionic Pt was also unsuccessful. A series of biotic and abiotic incubation experiments was conducted to investigate the hypothesis that these differences in mobility are driven by interactions with microbiota. Biofilms consisting of metallophilic bacteria formed on ultraflat Au surfaces and caused significant surface transformations. In contrast, only subtle changes were observed on Pt surfaces incubated under similar conditions. Minimal inhibitory concentrations for Au complexes are more than an order of magnitude lower than those measured for Pt complexes in *Cupriavidus metallidurans* cells. This higher cell-toxicity of mobile Au-compared to Pt-complexes can lead to toxic levels of mobile Au in the vicinity of Au grain surfaces. The elevated toxicity drives the formation of Au-detoxifying biofilms that catalyze the biomineralization of spheroidal nano-particulate and bacteriomorphic Au. In contrast, this does not occur on isoferroplatinum grains due to the lower toxicity of Pt. In conclusion, these results are consistent with microbial adaptation to element toxicity driving the cycling of precious metals in surface environments.

1. Introduction

It is commonly understood that microorganisms drive the cycling of metals that are essential for microbial nutrition or utilized to obtain metabolic energy (*e.g.*, Ehrlich, 1998; Southam and Saunders, 2005; Gadd, 2010). Recent research shows that microbes also affect toxic, rare and unessential metals; however, it is not known if microbial interactions with these metals are a major driver determining their mobility in surface environments (Southam and Saunders, 2005; Reith et al., 2012a). The dispersion of metals around ore deposits undergoing weathering is important for mineral exploration, because secondary metal mobility mediated by physical, chemical and biological agents can lead to the formation of geochemical halos in soils and deeper regolith materials, and hence expand the exploration footprint of ore deposits (Brugger et al., 2010; Hough et al., 2011). For example, Au is highly mobile in many near-surface environments, *e.g.*, calcrete,

* Corresponding authors at: The University of Adelaide and CSIRO Land and Water, Waite Laboratories, PMB2 Glen Osmond, 5064, South Australia, Australia. Tel.: +61 8 8303 8469; fax: +61 8 8303 8550.
E-mail addresses: joel.brugger@adelaide.edu.au (J. Brugger), frank.reith@csiro.au (F. Reith).

0009-2541/$ – see front matter © 2013 Elsevier B.V. All rights reserved.
http://dx.doi.org/10.1016/j.chemgeo.2013.02.010

soils and plants, leading to the formation of geochemical halos around hypogene Au deposits and the crystallization of high purity secondary Au (Reith et al., 2007; Hough et al., 2008). This mobility makes the sampling of weathered materials an effective exploration tool (*e.g.*, Lintern and Butt, 1993; Petts et al., 2009; Etschmann et al., 2010; Reith et al., 2011), and can also lead to the formation of secondary metal deposits (McCready et al., 2003). In addition, the study of environmental mobility of precious metals serves as an analog for understanding the long-term mechanisms of metal dispersion and biological adaptation to anthropogenic metal contamination, particularly as more and more Au- and Pt micro- and nano-materials are used in technical applications, which at the end of their life cycles find their way into the environment (Wiesner et al., 2006).

The role of biota in Au cycling has long been ambiguous (*e.g.*, Watterson, 1992, 1994), but recently progress has been made in understanding the role of microbiota in the interplay of processes leading to Au dispersion and re-concentration in surface environments (Reith et al., 2007; Southam et al., 2009). Recent advances include: (i) the detection of viable biofilms containing metal-resistant bacteria, *e.g.*, *Cupriavidus metallidurans*, on Au grains from a number of Australian locations (Reith et al., 2006), (ii) first insights into molecular-level processes of Au-microbiota interaction (Lengke and Southam, 2006; Lengke et al., 2006; Reith et al., 2009), (iii) the description of specific biochemical Au-resistance mechanisms in bacteria (Checa et al., 2007; Reith et al., 2009), and (iv) development of an integrated (bio)geochemical processes model for the (trans)formation of Au grains in surface environments (Reith et al., 2010; Fairbrother et al., 2012). In particular, nano- and micro-particulate and bacteriomorphic secondary Au have been shown to be diagnostic for the occurrence of biogeochemical transformations under surface conditions (Lengke et al., 2006; Reith et al., 2010, 2012a; Fairbrother et al., 2012).

In contrast to Au, only limited Pt mobility has been observed in many weathering environments, with surface concentrations in many Pt-bearing soils considered to be the result of physical rather than (bio)geochemical enrichment (*e.g.*, Cook and Fletcher, 1994; Fletcher et al., 1995; Hattori and Cameron, 2004), although residual accumulation can be associated with changes in Pt mineral speciation (Gray et al., 1996; Suárez et al., 2010). In combination with evidence for the maturation of Pt minerals in placer deposits (Cousins and Kinloch, 1976; Cabri et al., 1996), this suggests that Pt behaves differently to Au during weathering, and that Au mobility in surface environments is driven by processes that do not apply to Pt.

In this study, we assess the hypothesis that the contrasting behavior of Au and of Pt in surface environments is driven on the most fundamental level by differences in the biological toxicity of mobilized Au *versus* Pt. First, we assess the different mobility of Au and of Pt within a 10 mm-sized fragment of ferruginous paleochannel material, which contains abundant native Au- and isoferroplatinum grains. This unique, freshly collected sample provided a 'natural laboratory' to investigate the mobility of Au and Pt over geological times under environmentally identical conditions. Subsequently, we conducted experiments to assess the toxicity of important Pt and Au complexes on the metallophilic bacterium *C. metallidurans*, and the effects of biofilms of this and another metallophilic bacterium on ultraflat Au- and Pt surfaces.

2. Description of field sites and sample collection

Fifield is one of the few localities in the world where primary Au and Pt mineralization as well as placer Au and Pt occur together; thus a direct comparative analysis of fundamental drivers of Au and Pt cycling in natural surface environments can be conducted. The Fifield Pt–Au Field is situated about 380 km WNW of Sydney (New South Wales, Australia). It is the most productive placer deposit of Pt in Australia: 650 kg of alluvial Pt and 325 kg of alluvial Au were recovered from Early Tertiary deep leads, Pleistocene gravel and residual soils since its discovery in 1887 (Johan et al., 1989). The Fifield Pt–Au Field is part of the "Fifield Platinum Province", which contains 15 to 40 Alaskan–Uralian-type mafic-ultramafic intrusions that are made up of monzodiorite, gabbro–norite, hornblendite, hornblende/olivine/biotite/magnetite–clinopyroxenite, peridotite and dunite complexes. These ultramafics are Late Ordovician to Siluro-Devonian in age and intrude into Cambro-Ordovician metasediments as well as locally into Silurian and Devonian volcanics and sediments (Johan et al., 1989; Slansky et al., 1991; Crawford et al., 2007). Two types of primary PGE (platinum-group elements) mineralization have been recognized. Beside Pt–Fe alloys (tetraferroplatinum and isoferroplatinum), the pegmatitic pyroxenites of the Owendale complex contain a number of Os-, Pt- and Pd-sulfides and -antimonides. In contrast, mineralization associated with chromite-rich layers within dunites is dominated by isoferroplatinum with small inclusions of osmium–iridium alloys, and rare inclusions of Ru-, Rh- and Ir-sulfides (Johan et al., 1989; Slansky et al., 1991). The mineralogy and morphology of PGE within this latter type of mineralization corresponds more closely to the association found in the placer deposits, and the sample studied here was probably derived from this mineralization style. Platinum group minerals and Au nuggets have been concentrated into a number of deep leads (*e.g.*, Fifield, Gillenbine and Platina Leads) and also occur in soils overlying brecciated veins or fault zones. While the origin of PGE-minerals in placers is well described, the origin of the Au nuggets in placers is poorly understood, but may be attributed to nearby hydrothermal deposits.

The climate at Fifield is semi-arid, with most plant growth in summer, and temperature limiting growth in winter. Soils are classified according to Northcote (1979) as red podsols. The regolith over the Platina lead is a Pt–Au-bearing residual soil with limited iron pisolithic pebble development. Locally, lateritic weathering profiles are preserved over the Alaskan–Uralian-type intrusions. The landscape evolution of the Fifield area commenced in the Early to Middle Devonian, and weathering, erosion and deposition have continued since then.

The aggregate assessed in this study was recovered from the Platina deep lead paleochannel system (32°50′33.48″S and 147°28′5.38″E), which is assumed to be of Early Tertiary age. This sample was obtained using the field-sterile sampling procedures described in Reith et al. (2010). Groundwater samples were collected from two bores located up and downstream of the aggregate sampling site at 32°49′26.93″ S, 147°28′32.49″ E, and 32°50′39.12″ S, 147°28′4.41″ E, respectively. Groundwater samples were collected at approximately 30 m depth using a down-hole electric pump. Samples were collected from the first flush in Bores 1 and 3 as well as 2h after pumping of Bore 1.

3. Methods

3.1. Micro-analyses of the Pt/Au-aggregate

The aggregate and additional Au and Pt grains were mounted on C tape and analyzed using a FEI Helios NanoLab Focused Ion Beam Secondary Electron Microscope (FIB–SEM; FEI, Netherlands). Images were obtained at 3 to 15 kV with sectioning and cleaning carried out at 30 kV/21 nA and 30 kV–20 kV/2.8–0.34 nA. The instrument is equipped with a 10 mm^2 sapphire Si(Li) energy dispersive spectrometer (SEM-EDXA). Samples for SEM-EDXA were C-coated (3 nm) prior to analysis to negate charging issues resulting in local distortion of images for non-conducting materials. The aggregate was also investigated without C-coating to assess the presence of possible artifacts relating to the coating; no evidence for such artifacts was observed.

Synchrotron-based X-ray fluorescence micro-spectroscopy (SXRF) is very well suited for tracking rare particles of Au and Pt in complex geological materials (Etschmann et al., 2010), because of high sensitivity, μm-scale horizontal resolution, and the ability to sample a significant depth within the sample (*e.g.*, 50% of Au L X-rays escape the sample from a depth of 14 μm in goethite). For X-ray imaging, the sample was embedded in epoxy resin and polished using 1 μm

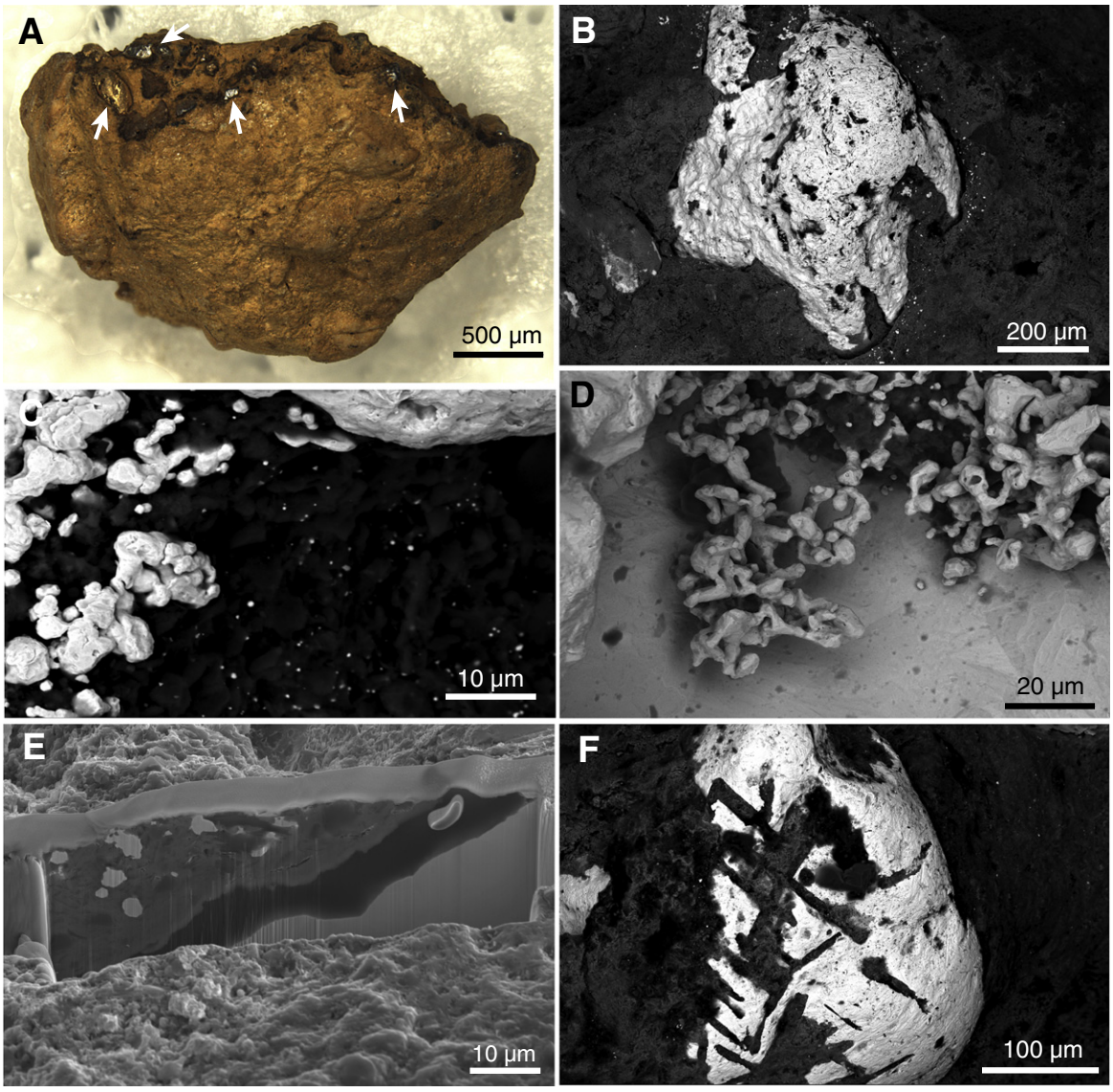

Fig. 1. Imaging of Au and isoferroplatinum grains from the Platina Lead at Fifield. (A) Optical image of the aggregate as retrieved; arrows point to Au (yellow color grain on the left side) and isoferroplatinum (white color grains) grains at the surface. (B) SEM image (Back Scattered Electron, BSE, mode) of one of the outcropping Au grains. Note the dusting of Au particles on the right side of the grain. (C) Detail of Au particles occurring within the sediment next to a Au grain (edge visible on top). Both sub-μm particles and μm-size aggregates exist. (D) SEM image (BSE mode) of bacteriomorphic Au on a Au grain. (E) FIB section through the regolith material overlying a shallow Au grain. (F) SEM image (BSE mode) of one of the outcropping isoferroplatinum grains. The herringbone inclusions consist of weathered out inclusions of iridosmine.

diamond paste. X-ray fluorescence data for 10 serial cuts (~100 μm polishing at each step) were collected at the XFM beamline at the Australian Synchrotron in Melbourne, Australia. The XFM beamline is an undulator beamline with a Si(111) monochromator and an energy resolution ($\Delta E/E$) of 2×10^{-4} at 10 keV. Kirkpatrick–Baez mirrors were used to focus the beam to a spot size of ~1.5 μm^2. Fluorescence data were collected using the massively parallel 384-element MAIA detector system (Ryan et al., 2010a, 2010b). The detector was placed in front of the sample at a distance of 2 mm, which enables the collection of nearly 50% of a full hemisphere of the X-rays emitted by the sample. The incident X-rays traveled through a central hole in the detector. The SXRF data were analyzed with GeoPIXE II (Ryan et al., 2005) using the dynamic analysis (DA) method to project quantitative elemental images from the full fluorescence spectra (Ryan, 2000; Ryan et al., 2009). The DA technique is a matrix transform algorithm that unfolds overlaps and subtracts background, escape peaks and other detector artifacts. The advantage of this technique is that by fitting multiple lines per element, the method benefits from better counting statistics and it is possible to distinguish between elements that have overlapping X-ray lines, which are traditionally difficult to separate using the region of interest approach.

X-ray absorption near-edge structure (XANES) spectra at the Pt L_3 edge (11564 eV) are sensitive to the oxidation state of Pt; in particular, Pt(IV) salts show high white lines compared to metallic Pt and Pt(II) salts (Hall et al., 2003). We used the XANES imaging method (Etschmann et al., 2010) to hunt for particles containing ionic Pt. μ-XANES is a powerful method to identify the presence and distribution of minor species in complex specimens, and is usually performed by collecting spectra from a few regions of interest (*e.g.*, Brugger et al., 2008; Lintern et al., 2009). This approach has a number of problems, including the challenge of finding rare components from the analysis of a limited number of points; operator bias in the selection of these points; and the possibility of beam damage. To overcome these limitations, some authors have collected elemental maps at a few monochromatic energies in order to obtain some information regarding speciation

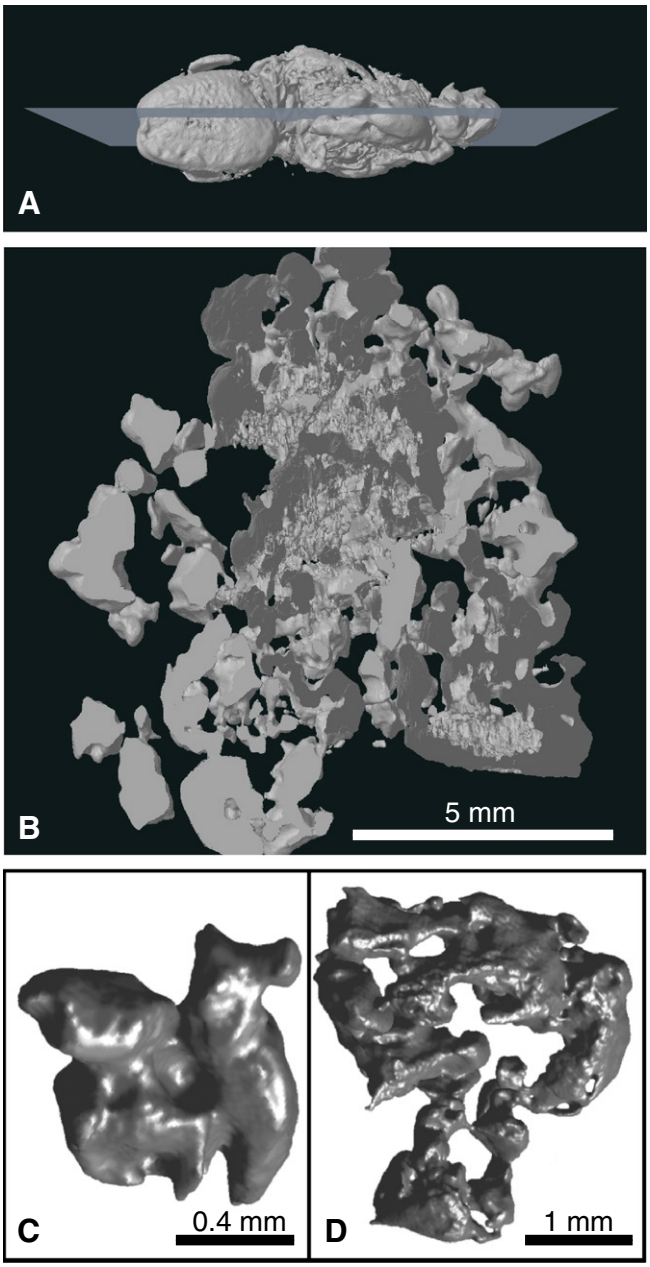

Fig. 2. X-ray tomography of the Au–Pt aggregate from Fifield. (A,B) Reconstruction of the Au and isoferroplatinum grains in the aggregate, revealing a high proportion of these grains. (A) is an overview, (B) a cut along the plane shown in (A). Morphology of single isoferroplatinum (C) and Au (D) grains extracted from the model shown in (A, B).

distribution (Martinez-Criado et al., 2005; Denecke et al., 2007; Mayhew et al., 2011). This approach has proven invaluable for indentifying rare components with a spatially limited distribution (Etschmann et al., 2010), especially with the advent of fast X-ray detectors that provide a quantum leap in data acquisition rate and open the way to megapixel SXRF imaging (*e.g.*, MAIA detector; Lombi et al., 2011; Ryan et al., 2009). XANES imaging is well-suited for the study of the aggregate from Fifield: a spatially resolved technique is required, because of the necessity to identify metallic Pt; ionic Pt may exist both as discrete phases (*e.g.*, Pt-oxides and hydroxides) or sorbed on mineral surfaces (Butt et al., 2001); and tetravalent Pt has a characteristic large white line.

Standard XANES (11540 to 11600 eV, 0.5 eV step) were measured on a Pt-foil and a PtO_2 pellet diluted with BN to determine the monochromator energy offset and select relevant energy points for the XANES stack. Stacks of full-spectral SXRF maps (XANES stack) were collected at seven irregularly spaced monochromator energy points from 11.60 to 11.54 keV spanning the Pt L_3 edge (11.6, 11.5695, 11.568, 11.5665, 11.565, 11.5635, 11.54 keV). An area of 3.818×1.612 mm^2 was scanned continuously at a rate of 1.02 mm s^{-1} with a pixel dwell time of 1.953 ms, using a pixel size of 2×2 μm^2 and a beam size (focused with slits) of 2×8 μm^2. The resulting XANES stack consisted of seven images of 1.54×10^6 pixels each. To construct XANES stacks, the SXRF spectrum at the highest monochromator energy (11.60 keV) was fitted in GEOPIXE II, a DA matrix was formed, and the quantitative images for Pt and the other detected elements were extracted. The following Pt SXRF maps, collected at lower monochromator energies, were extracted using the DA matrix obtained for the highest energy image. The Pt and Fe images were exported from GeoPIXE II, and aligned using the ImageJ package (Abramoff et al., 2004). The transformation matrices were determined using the Fe images, since the small differences in beam energy among images do not significantly affect the Fe fluorescence yields, and the Pt images were corrected using these transformation matrices. We used the SIFT correspondence algorithm to automatically pick points for alignment, and then *bUnwarpJ* (Arganda-Carreras et al., 2006) to align the images. The aligned images were read into MATLAB for further analyses.

The composition of the aggregate was also mapped using a Cameca SX50 electron microprobe (EMP; Cameca, France) after coating the sample with a 15 nm thick C film. The EMP can access X-ray lines (*e.g.*, Ag L) that are outside the detection range of the MAIA detector. Data collection and reduction were performed with the SAMx package. Analyses were conducted at 20 kV and 19.9 nA with a 1 μm beam diameter. The grains were analyzed for (typical detection limits in parenthesis as wt.%): Al (0.06), Si (0.05), S (0.05), Fe (0.08), Ni (0.09), Cu (0.11), As (0.25), Pd (0.25), Ag (0.25), Au (0.28), Hg (0.6) and Bi (0.5). All the elements were calibrated on a mixture of minerals and pure metal standards from Astimex.

3.2. X-ray micro-tomography

X-ray micro-tomography is a non-destructive technique used for the visualization of the internal structure of samples. A high-resolution desktop X-ray micro-CT-system (SkyScan 1072, SkyScan, Belgium) with a closed X-ray micro-focus source was used. A 1 mm Al filter was used to obtain better contrast and to reduce beam hardening artifacts. The peak voltage of the source was set at 100 kV and 100 μA current. Projection images were acquired with a rotation step of 0.45° over 180° and the signal to noise of the projection images was improved by averaging 3 frames. The cross sections were reconstructed using a cone-beam algorithm (NRecon software, Skyscan).

3.3. Chemical analyses of natural water samples from Fifield

Water samples were analyzed for pH (Rayment and Higginson, 1992) on site, and for electrical conductivity (APHA method 2510) and alkalinity (APHA method 2320) in the laboratory. Dissolved carbon was determined by APHA method 5310 B on a Skalar Formacs HT TOC/TN Analyzer. Inorganic carbon was acidified to form CO_2 prior to detection. Dissolved organic carbon was determined by the difference between total and inorganic C. Total N was determined at the same time as total C on the dual detector instrument. Ammonia-nitrogen (NH_4-N) was determined by flow analysis and spectrometric detection according to ISO 11732. Nitrate- and nitrite-N were determined by APHA method 4500-NO_3-F using the automated segmented flow analyzer (Alpkem Flow Solution 3) at 540 nm. The NO_3-N (also referred to as NO_X-N indicating the sum of nitrite and nitrate nitrogen) concentration was calculated from a set of calibration standards measured at the same time. Anions (F^-, Cl^-, NO_2^-, Br^-, NO_3^-, SO_4^{2-} and PO_4^{3-}) were measured by the APHA method 4110 using a Dionex ICS-2500 ion chromatography system with 2 mm AS16 anion separation column.

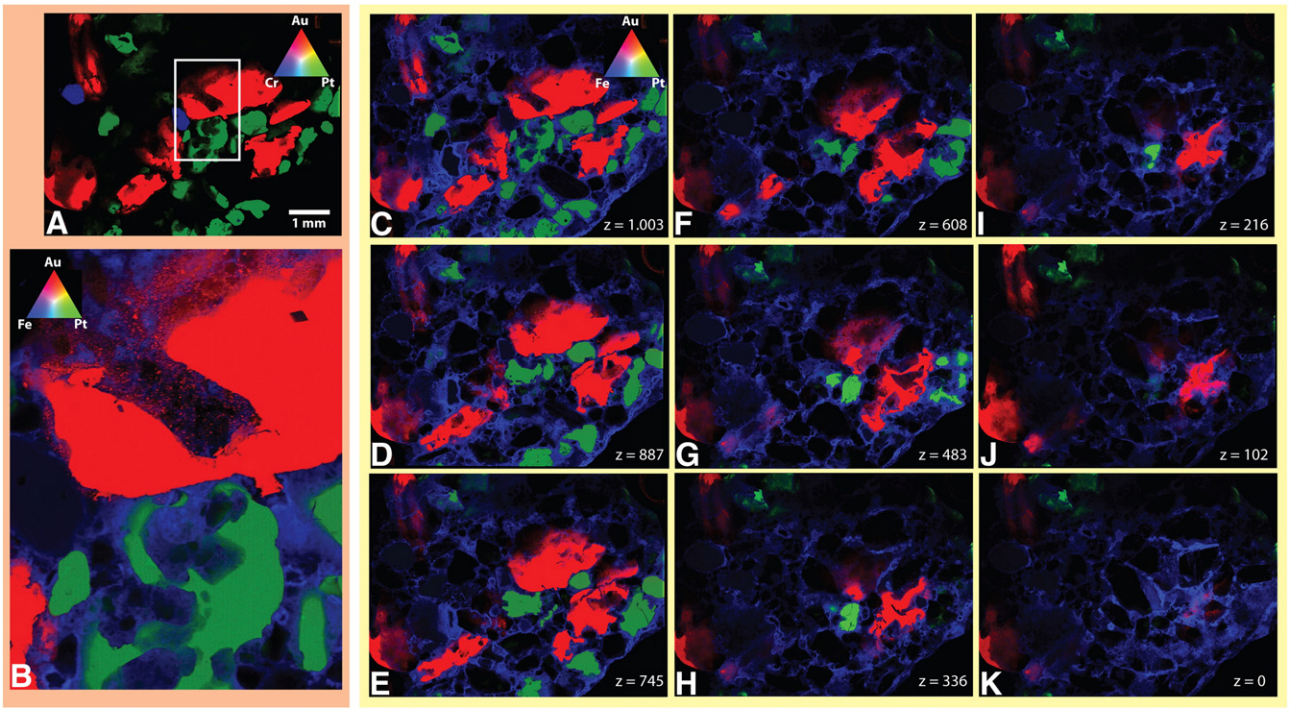

Fig. 3. Results of μ-XRF chemical imaging of serial sections through the aggregate from Fifield using the MAIA massively parallel X-ray detector, shown in the RGB (red–green–blue) color space. (A) RGB (Au–Pt–Cr) image of the deepest section. (B) Detail RGB (Au–Pt–Fe) image, showing particulate Au remobilization and embayments corresponding to weathered out olivines in the isoferroplatinum. (C–K) RGB (Au–Pt–Fe) Images as a function of the polishing depth, z (in μm).

The cations and metals were determined by APHA method 3120 using inductively coupled plasma optical emission spectroscopy (ICP-OES) on a Spectro ARCOS (Spectro Analytical Instruments, Kleve, Germany). Trace and ultratrace elements were analyzed by inductively coupled plasma mass spectrometry (ICP–MS; Agilent 7500ce, USA); quantification limits are given in Table 2.

3.4. Geochemical modeling

Calculations were conducted using the Geochemist's Workbench (GWB; Bethke, 2008). GWB was remote controlled by a MATLAB custom-code; MATLAB was also used to generate the graphics. Thermodynamic properties were taken from the Lawrence Livermore National Laboratory database (version R9), with properties for Au and Pt complexes updated as follows: properties for Au(I) and Au(III)-chloride, -hydroxide and -bisulfide complexes selected by Usher et al. (2009); Pt(II)-bisulfide complexes from Gammons and Bloom (1993) and Pan and Wood (1994), following Barnes and Liu (2012); Pt(II)-chloride complexes from Wood et al. (1992); Pt(IV)-chloride complexes from Gammons (1995); Pt(II) thiosulfate complexes from Hancock et al. (1977); $Pt(OH)_2(aq)$, $Pt(OH)^+$, PtS(s) and $PtS_2(s)$ from Sassani and Shock (1998); and PtO(s) and $PtO_2(s)$ from Inzelt and Horányi (2006).

3.5. Microbial experiments

The minimal inhibitory concentration (MIC), defined as the lowest concentration inhibiting bacterial growth, is used as a standard measure for the resistance of microorganisms to metal ions and complexes as well as other antimicrobial agents (Nies, 1999). As a result, conclusions can be drawn about the relative toxicity of these compounds towards the species tested (Nies, 1999). MICs for Au- or Pt-salts in *C. metallidurans* CH34 were determined in triplicate on solid TrisMM containing 2 g sodium gluconate L^{-1} and 20 g agar L^{-1} (Mergeay et al., 1985). A pre-culture of *C. metallidurans* CH34 was incubated at 30 °C and 250 rpm for 30 h until early stationary phase, then diluted 1:20 in fresh medium and incubated for 24 h at 30 °C and 250 rpm until exponential phase. This exponential phase culture was diluted 1:100 in fresh medium and used for streaking onto plates containing 0–250 μM of the respective Au- or Pt-salts. The plates were incubated at 30 °C for 120 h, and cell growth was monitored as ability to form colonies.

Ultra-flat Au- and Pt platelets sized 5×5 mm^2 were prepared from 99.95% Au and Pt foils (Strem Chemicals, USA). These foils were annealed at 800 °C for 16 h following the procedures described in Fairbrother et al. (2009). A pattern of five boxes, each 20×20 μm^2 in size, was FIB-milled onto the surface of each platelet using a FIB–SEM with an ion beam operated at 30 kV and 2.8 nA. Sterilized Au and Pt platelets were then incubated in triplicate in 25 mL growth medium containing 1:1 peptone-meat extract (PME, 13 g per liter; pH 7, Difco, USA), inoculated with *Chromobacterium violaceum* or *C. metallidurans* CH34. Flasks were inoculated with 2% of pre-culture from an exponential phase culture (OD600 = 0.58), and incubated standing upright at 25 °C in the dark for up to 56 days. Sterile control experiments containing Au and Pt platelets and medium but no cells were also conducted. Samples were collected at days 1, 7, 14, 21, 28 and 56 in experiments with viable cells and at days 1, 14, 28 and 56 in sterile controls. Throughout the experiments viable cells were counted on PME agar plates (17.5 g L^{-1} Water, Difco, USA) following the method of Miles and Misra (1938). Cell growth in the medium was also monitored *via* OD measurements using a Klett-Summerson-Colorimeter (Klett MFG Co., USA). At each sampling time the remaining vials were amended with 0.5 mL of a concentrated PME solution (80 g L^{-1}). This led to periodically nutrient-rich (*i.e.*, a 20% supplement of the original media constituents) conditions that should extend the metabolic activity and viability of the cultures, followed by the induction of cyanide formation when nutrient availability becomes limited.

Biofilm development on selected Au or Pt platelets at days 1 and 56 was examined using staining with an acridine orange stain (20 μL, Sigma, USA). Double-stranded nucleic acids fluoresce green and single-stranded nucleic acids emit orange–red fluorescence when stained with acridine orange (Kepner and Pratt, 1994). The

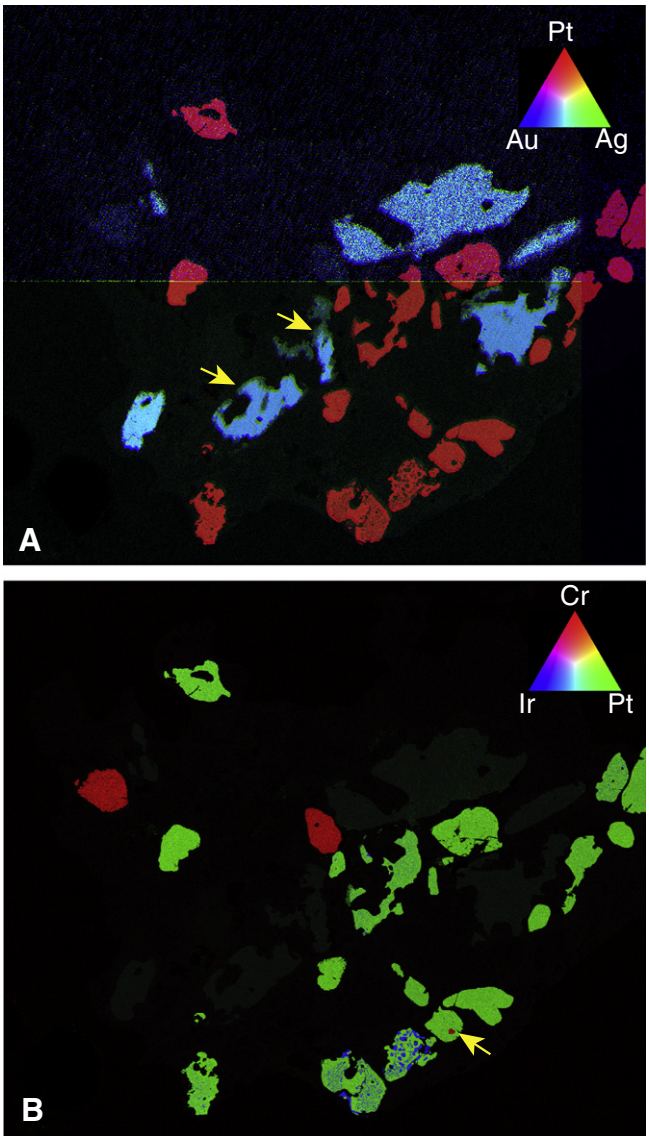

Fig. 4. Electron microprobe maps of the sample (polishing depth z = 1003 μm), showing (A) zones of Ag-depletion around the Au grains (arrows), and (B) inclusions of chromite (arrow) and iridosmine (blue inclusions) within isoferroplatinum grains.

Au or Pt platelets incubated with the bacteria were placed on a glass slide and acridine orange stain was added. After a 2 minute incubation period, the platelets were washed with MilliQ water, covered with a cover slip and imaged using a fluorescence microscope (Nikon Eclipse, Nikon, Japan), and biofilm development was observed (data not shown).

The surfaces of the platelets were examined further following the procedures described in Fairbrother et al. (2009). Gold and Pt foils were collected under aseptic conditions and sonicated for 40 min in a beaker to clean the surfaces of adhering *C. metallidurans* and *C. violaceum* cells and other biofilm components (*e.g.*, exopolymeric substances) prior to electron microscopic analyses. To avoid overheating the sample, sonication was conducted in a 160HT Soniclean sonicator (Soniclean Benchtop Ultrasonic Cleaners Pty., Adelaide, Australia) holding 1 L of deionized water. Scanning electron microscopy of platelets was conducted before and after sonication to image the biofilms, as well as check the efficiency of the sonication procedure. The samples were studied with a FIB–SEM at an acceleration voltage of 5 kV. For the measurements of Au and Pt concentrations in the medium, the 56-day culture samples were acidified to 5 wt.% HCl, and analyzed using the He mode in an octopole reaction system with an Agilent CX ICP–MS (Agilent Technologies, CA, USA). The quantification limits for Au and Pt were 0.2 μg L^{-1}.

4. Results and discussion

4.1. Distribution of Au and Pt in the Fifield aggregate

The 10 × 5 × 5 mm aggregate contained abundant Au and isoferroplatinum grains, of which some were outcropping (Fig. 1A). X-ray tomography confirmed that Au and isoferroplatinum grains occupied a significant volume of the aggregate (Fig. 2A, B). The grains were cemented into an Fe-oxide-rich matrix, also containing well-rounded quartz grains. SEM and X-ray tomography of the unprocessed aggregate showed that the Au grains displayed complex morphologies, with high purity secondary Au rims, and abundant dissolution and accretion morphologies, including spheroidal and bacteriomorphic Au (Figs. 1C, D; 3B). This shows that the grains were transformed in the surface environment and suggests that biogeochemical processes catalyzed these transformations (Reith et al., 2010). Similar Au morphotypes were also observed in two recent studies of Au grains from (semi-)arid and temperate sites in Australia and New Zealand, respectively, and were shown to be indicative for the occurrence of biogenic transformations (Fairbrother et al., 2012; Reith et al., 2012b). The most striking feature of the SEM and SXRF analyses of the untreated grains was a dusting of fine-grained particulate Au in matrix materials surrounding the Au grains. This dusting displayed its highest density within ~50 μm of the Au grain surfaces (Figs. 1B, C; 3), consisted of high purity metallic Au, and comprised both nano-particles and μm-scale aggregates ranging in sizes from <10 nm to >10 μm in diameter (Figs. 1C, D, 3B). FIB-sectioning confirmed that these Au particles occurred throughout the sedimentary material (Fig. 1E). In particular, the MAIA X-ray fluorescence maps provide a stunning view of the dispersion of Au particles around Au grains (Fig. 3). The distribution of the Au particles was not homogeneous around the sample, often being limited to one side of the Au grain (*e.g.*, Fig. 3B). This may reflect the differences in porosity of the matrix, but could also be linked to fluid- and nutrient flow in the groundwater system that harbored the aggregate. Overall particle sizes and morphologies are similar to those observed on Au grains from New Zealand, where a significant dispersion of nano- and microparticles of Au into the soil matrices surrounding the grains was also observed (Reith et al., 2012b). In New Zealand a particularly strong effect was observed on grains from the West Coast of the South Island, which was linked to the higher availability of water sustaining a higher biological activity at those sites.

In contrast, isoferroplatinum grains were smooth, well-rounded (Fig. 1F), and based on FIB–SEM investigations of the grain surfaces, no unequivocal evidence for Pt dissolution was apparent. The grains contain a number of embayments that were often ovoid (Figs. 2C, 3B), and sometimes herringbone-like in shape (Fig. 1F). The former correspond to weathered out olivine grains, the latter to weathered out iridosmine (Johan et al., 1989). In addition, some isoferroplatinum grains also contained preserved chromite grains (Figs. 3A, 4B). Detailed examination of Pt grain surfaces and matrix materials enrobing the grains using FIB–SEM and SXRF did not reveal nano- or μm-scale metallic Pt particles (Fig. 3).

As no nano-particulate Pt was observed in the Platina deep lead aggregate, μ-XANES spectroscopy was used to assess the presence of other Pt-species that would indicate the Pt mobility. Maps of the intensity of the white line, based on the ratios of the intensities measured at the while line energy (11568 eV) and that at the highest measured energy (11600 eV), did not reveal particles containing ionic Pt (Fig. 5B). Pixels displaying white line intensities higher than that of metallic Pt are located near the rim of the isoferroplatinum grains; careful examination of the XANES data at those points showed no evidence for ionic

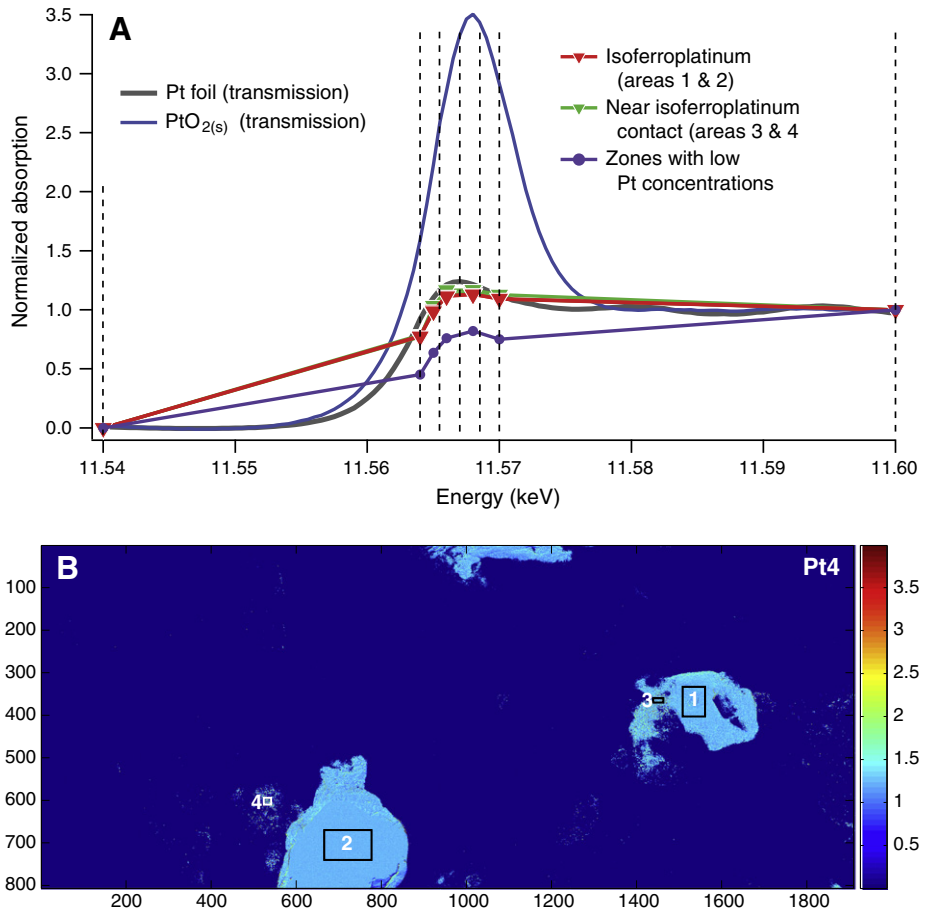

Fig. 5. Results of XANES imaging. (A) Extracted XANES spectra compared to the spectra measured in transmission mode on a metallic Pt foil and on PtO_2 powder. The areas for the extracted spectra are shown in B. Note that the smaller intensity of the white line for the spectra obtained on isoferroplatinum, compared to the metallic Pt standard, is due to self-absorption affecting the fluorescence measurements. (B) Map of the relative intensity of the white line at 11568 eV.

Pt either, but rather indicated that the anomalous values were due to approximately 2 μm misalignments in the images, that resulted in significant discrepancies between the intensities measured for these pixels in subsequent maps, as Pt concentrations vary by orders of magnitude over a few pixels. This was confirmed by the spectra obtained from the integration of counts within small regions containing many anomalous pixels (regions 2 and 3, Fig. 5B), which are similar to those obtained on the isoferroplatinum (Fig. 5A). Overall, these data showed no evidence of ionic Pt on the surface of the isoferroplatinum grains or within the ferruginous material between the grains (Fig. 5).

4.2. Solubility of Au and Pt in Fifield-type groundwaters

While Pt mobility was not observed, large amounts of Au were redistributed throughout the sample as metallic nano- and microparticles. A fundamental problem in understanding Au and Pt mobility in the weathering environment is related to understanding the relative influences of biogenic and abiogenic factors (*e.g.*, Hough et al., 2008; Lintern et al., 2009; Reith et al., 2010, 2011). In order to assess the capacity of inorganic ligands to differentially mobilize Au and Pt at Fifield, we used equilibrium thermodynamics to calculate

Table 1
Results of geochemical analysis of the groundwater from Fifield: pH, electrical conductivity (E.C.), ammonia-nitrogen (NH_4-N), the sum of nitrate- and nitrite-nitrogen (NO_x-N), nitrite-nitrogen (NO_2-N) total nitrogen (TN), total alkalinity, dissolved carbon (DC), inorganic carbon (IC), dissolved organic matter (DOC), and major anions.

	pH	E.C.	NH_4-N	NO_x-N	TN	Total alkalinity	DC	IC	DOC
Units		dS m^{-1}	mg L^{-1}	mg L^{-1}	mg L^{-1}	meq L^{-1}	mg L^{-1}	mg L^{-1}	mg L^{-1}
Detection limits	–	0.01	0.005	0.005	0.1	–	0.5	0.1	0.5
Bore 1	7.97	21.69	0.012	0.19	0.23	10.084	120.25	104.19	16.06
Bore 1 (recharge)	8.09	19.98	0.054	0.19	0.33	10.084	117.27	102.22	15.05
Bore 3	8.15	17.37	0.41	0.05	0.48	7.82	109.3	94.36	14.94

	[a]Cl^-	[a]Br^-	[a]NO_3^-	[a]$SO_4^{=}$	[b]Ca	[b]K	[b]Mg	[b]Na	[b]S	[b]Si	[b]Sr
Units	mg L^{-1}	mg L^{-1}	mg L^{-1}	mg L^{-1}	mg L^{-1}	mg L^{-1}	mg L^{-1}	mg L^{-1}	mg L^{-1}	mg L^{-1}	mg L^{-1}
Detection limits	0.05	0.05	0.05	0.05	0.1	0.1	0.1	0.1	0.1	0.1	0.05
Bore 1	7900	28	2.4	4300	401	10.8	1090	4210	1340	4.02	7.77
Bore 1 (recharge)	8000	29	2.7	4300	395	22.3	1080	4230	1320	3.95	7.58
Bore 3	4700	14	3.2	4400	208	<1	341	3930	1360	9.48	3.4

Notes: NO_2-N<0.005 mg L^{-1}.
[a] Elements analyzed by ion chromatography; F^-<2 mg L^{-1}.
[b] Elements analyzed by ICP-OES; Al, As, Cd, Co, Cu, Mn, Mn, Ni, Pb, Se, Zn<0.5 mg L^{-1}; B, Fe, P, Sb<1 mg L^{-1}.

Table 2
Results of geochemical analysis of the groundwater from Fifield: ICP–MS analysis of trace elements in μg L^{-1}.

	Cr	Fe	Co	Ni	Cu	Ga	Ge	As
Detection limits	0.2	0.2	0.2	0.8	0.2	0.04	0.2	0.5
Bore 1	0.63	<0.2	<0.2	1.2	<0.2	2.9	0.63	0.77
Bore 1 (recharge)	<0.2	5.7	<0.2	1.5	0.91	2.5	0.42	1.8
Bore 3	<0.2	<0.2	2.5	3.3	2.1	0.81	<0.2	11

	Se	Nb	Cd	Te	Sm	W	Au	Th	U
Detection limits	1	1	0.2	0.2	0.2	0.1	0.1	0.2	0.2
Bore 1	9.2	5.4	2	2.9	0.25	26	1.2	0.24	2.3
Bore 1 (recharge)	10	8.1	1.4	2.4	<0.2	100	1.7	0.29	3.7
Bore 3	<1	2.7	0.9	4.3	<0.2	15	<1	0.22	<0.2

Notes: Other elements analyzed by ICP–MS were below detection of 0.2 mg L^{-1} Sc, Zn, Y, Pd, Ag, La, Ce, Pr, Nd, Eu, Gd, Db, Dy, Ho, Er, Tm, Yb, Lu, Re, Pt, Pb.

the relative solubility of Au and Pt in Fifield-type waters (Tables 1, 2). The present-day groundwaters at Fifield are basic (pH ~ 8), and dominated by chloride and sulfate anions. Gold concentrations up to 1.7 μg L^{-1} were detected in the waters, and in contrast Pt concentrations were below detection limit (<0.2 μg L^{-1}). The results of the calculations are shown in Fig. 6, where they are plotted as a function of redox potential and pH in a solution with a composition similar to modern-day groundwater at Fifield. The diagrams in Fig. 6 were constructed by calculating the equilibrium composition of a water containing 7900 mg L^{-1} Cl, 4300 mg L^{-1} S as sulfate, 1.2 μg L^{-1} of each Au and Pt, and Na adjusted for charge balance, over a grid of pH and log $f\,O_2(g)$.

The calculated Au/Pt ratios show that Au can be much more soluble that Pt in some conditions, with ratios exceeding 10^{10} (Fig. 6A). However, the calculated Pt solubility can exceed that of Au under reducing conditions (hydrosulfide stable) at low or high pH (pH<5 or pH>9), and the Au and Pt concentrations are near equal in basic solutions at the HS^-/SO_4^{2-} redox buffer. Similarly, both metals are relatively soluble (>1 μg L^{-1}) under oxidizing conditions. At Fifield, redox conditions are likely governed by the sulfate/hydrosulfide buffer (basic pH ~ 8; sulfate in solution but H_2S smell), because the mineralization at Fifield is associated with sulfides. Biologically mediated sulfide oxidation produces a number of sulfur species with intermediate oxidation states, most prominently thiosulfate (Reith et al., 2007). Since thiosulfate is an excellent ligand for both Au and Pt (Benedetti and Boulègue, 1991; Anthony and Williams, 1994), we also conducted thermodynamic calculations assuming that the solution contains 2 mg L^{-1} metastable thiosulfate (Fig. 6D–F). The results show that the presence of thiosulfate does not significantly alter the solubility differential (Fig. 6A, D). Note that the inclusion of the small amounts of Br^- (14–29 mg L^{-1}) and ammonium (0.01–0.41 mg L^{-1}) quantified in the waters did not change the results of the thermodynamic modeling. Overall, these calculations suggest that differences between Au and Pt mobility are not only derived from differences in chemical solubility, because the chemical solubility of Au is little higher than that of Pt solubility under conditions relevant for Fifield (Fig. 6A, B).

4.3. Environmental toxicity of Au and Pt complexes and the formation of biofilms on precious metal surfaces

Thermodynamic modeling shows that under conditions likely to prevail in the groundwaters at Fifield, the solubility of both Au and Pt can exceed 1 μg L^{-1}. This suggests that the observed differences in mobility cannot only be related to these solubility differences. In order to assess whether biological toxicity can drive the observed differences in Au and Pt behavior, we measured the MICs for Au- and Pt-complexes in *C. metallidurans* CH34. The MIC of Au(III)-chloride and Au(I)-thiosulfate in TrisMM are 0.9 and 0.5 μM. In contrast, MICs for Pt-chloride complexes were 200 μM and 17.5 μM for Pt(II/IV)-chloride, respectively. These results show that Au(I/III)-complexes are several orders of magnitude more toxic to *C. metallidurans* than the Pt(II/IV)-complexes. Similar results were obtained in a study with *Escherichia coli*, here MIC values for Au(III)-complexes of 20 μM compared to 500 for Pt(IV)-complexes were measured (Nies, 1999).

Neither Pt nor Au exist as free ions in aqueous solution under surface conditions, but occur as metal complexes (Wood et al., 1992; Wood, 2002; Reith et al., 2007). The toxicity of these metal complexes towards cells is determined by how much of the metal complex is available to interact with the cells, which is largely determined by how stable these complexes are in aqueous solutions, and the affinity and capacity of cells for the sorption of these complexes (Nakajima, 2003). Modeling of Fifield waters indicated that the most likely Au and Pt species to occur under the prevailing conditions are complexes with chloride and thiosulfate (Fig. 6). Earlier work by Butt et al. (2001) has shown that Pt, if dissolved, forms highly stable chloride complexes in aqueous solutions under surface conditions that interact little with organic matter. In contrast, Au(III)-chloride complexes are labile and are rapidly adsorbed by living bacterial cells as well as inactive and dead cells (*e.g.*, Reith et al., 2007, 2009; Kenney et al., 2012; Song et al., 2012). This was confirmed in recent experiments, in which the uptake of Au(I/III)- and Pt(II/IV)-complexes in *C. metallidurans* was assessed. Results showed that across the range of pHs (5–8) tested, uptake of Pt-complexes by cells after 6 h and 144 h was commonly 30 to 70% lower compared to equivalent Au-complexes (Reith et al., 2009; Fairbrother, pers. comm.). These data strongly suggest that under otherwise identical conditions more Au complexes are likely to reach cells than Pt complexes. These Au complexes will then interact with the cells to block protein function and create oxidative stress (Reith et al., 2009). In order to reduce Au(I/III)- or Pt(II/IV)-complexes to their metallic forms 1 or 3 and 2 or 4 electrons, respectively, are required to be actively or passively transferred by the cells. As electron transfer reactions in electron transport chains of bacterial cells commonly occur in pairs of electrons, the reduction of Au-complexes likely leads to the formation of free electron radicals, further increasing oxidative stress and hence toxicity of Au in the cells (Nies, 1999).

The ability of bacterial biofilms to promote precious metal mobility and to explain the difference between Au and Pt was assessed using incubation experiments, in which the bacteria *C. violaceum* (cyanide-producing) and *C. metallidurans* (metallophilic) were incubated for up to 56 days on ultraflat Au- and Pt surfaces. Prior to exposure, Au and Pt surfaces were engraved with five $20 \times 20\ \mu m^2$ reference squares (*e.g.*, Fig. 7A). After exposure to the biofilms, SEM imaging revealed that the squares had disappeared from the Au plates, the surface of the Au platelets was intensely pitted, and a significant roughening of the surface had occurred (Fig. 7A–C). This shows that biofilm-mediated dissolution and re-precipitation of Au had occurred, as Au concentrations were below 10 μg L^{-1} in solution. In contrast, only subtle changes to the Pt surfaces were observed after the incubation (Fig. 7D–F), and no Pt was detected in the experimental solutions (<0.2 μg L^{-1}).

Active biofilms are commonly observed on Au grains from wet-(sub) tropical regions in Australia (Reith et al., 2006, 2010). In arid and semi-arid environments, biofilms formation also drives secondary Au

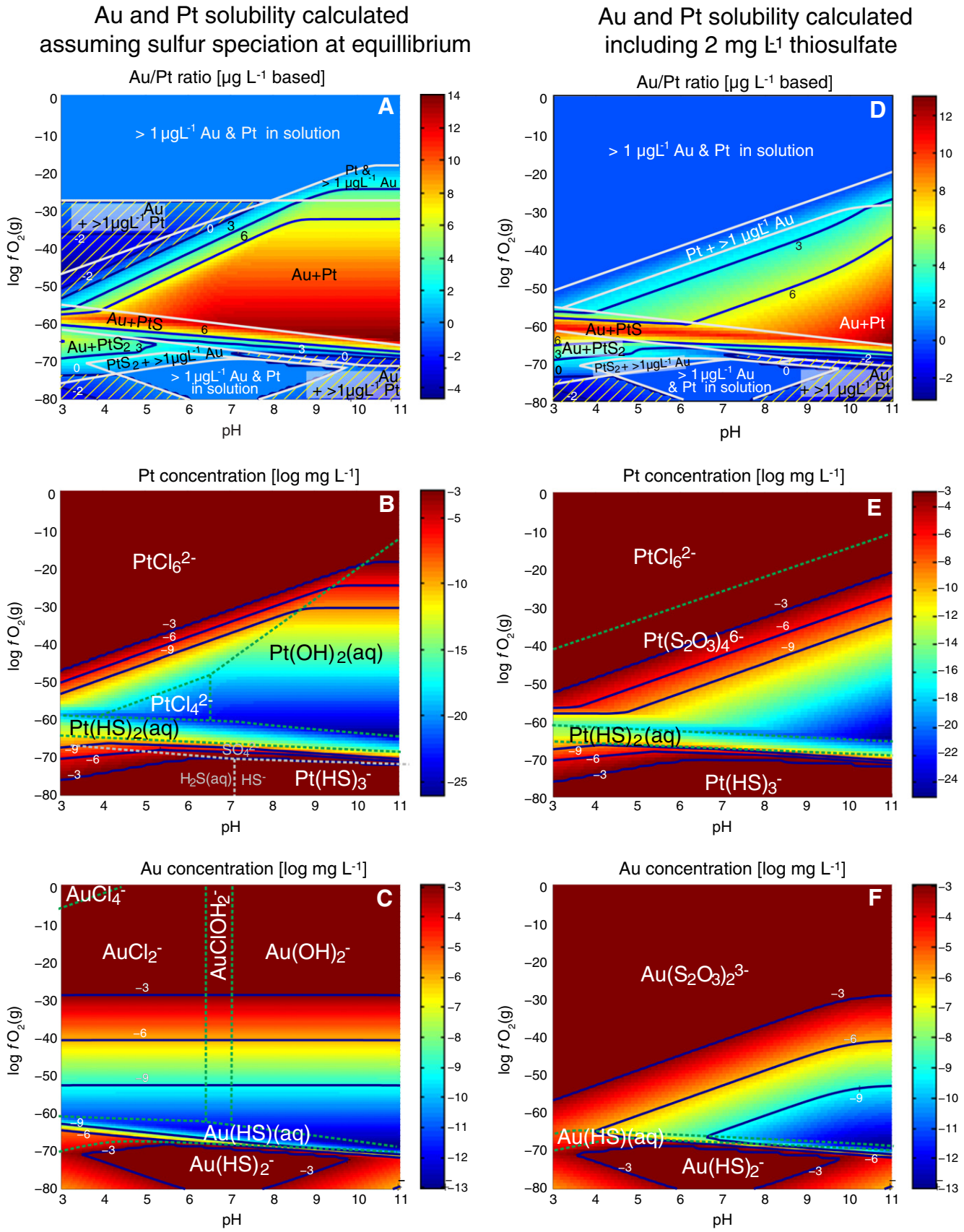

Fig. 6. Results of geochemical modeling comparing the solubility of Au and Pt in Fifield-type groundwater (7900 mg L^{-1} Cl, 4300 mg L^{-1} S as SO_4^{2-}), plotted as a function of redox potential and pH. Thermodynamic equilibrium is assumed for all elements in the calculations for Figures A–C; in contrast, for D–F, 2 mg L^{-1} metastable thiosulfate was added. The calculations represent the equilibrium assemblage in a closed system, with total amounts of Pt and Au available corresponding to 1.2 µg L^{-1}. (A, D) Ratio of Au over Pt (mg L^{-1}), plotted together with the minerals present in the system. Hatched areas correspond to conditions where Pt is more soluble than Au. (B, E) Concentrations of aqueous Pt, also showing the predominant Pt complexes. (F, G) Concentrations of aqueous Au, also showing the predominant Au complexes.

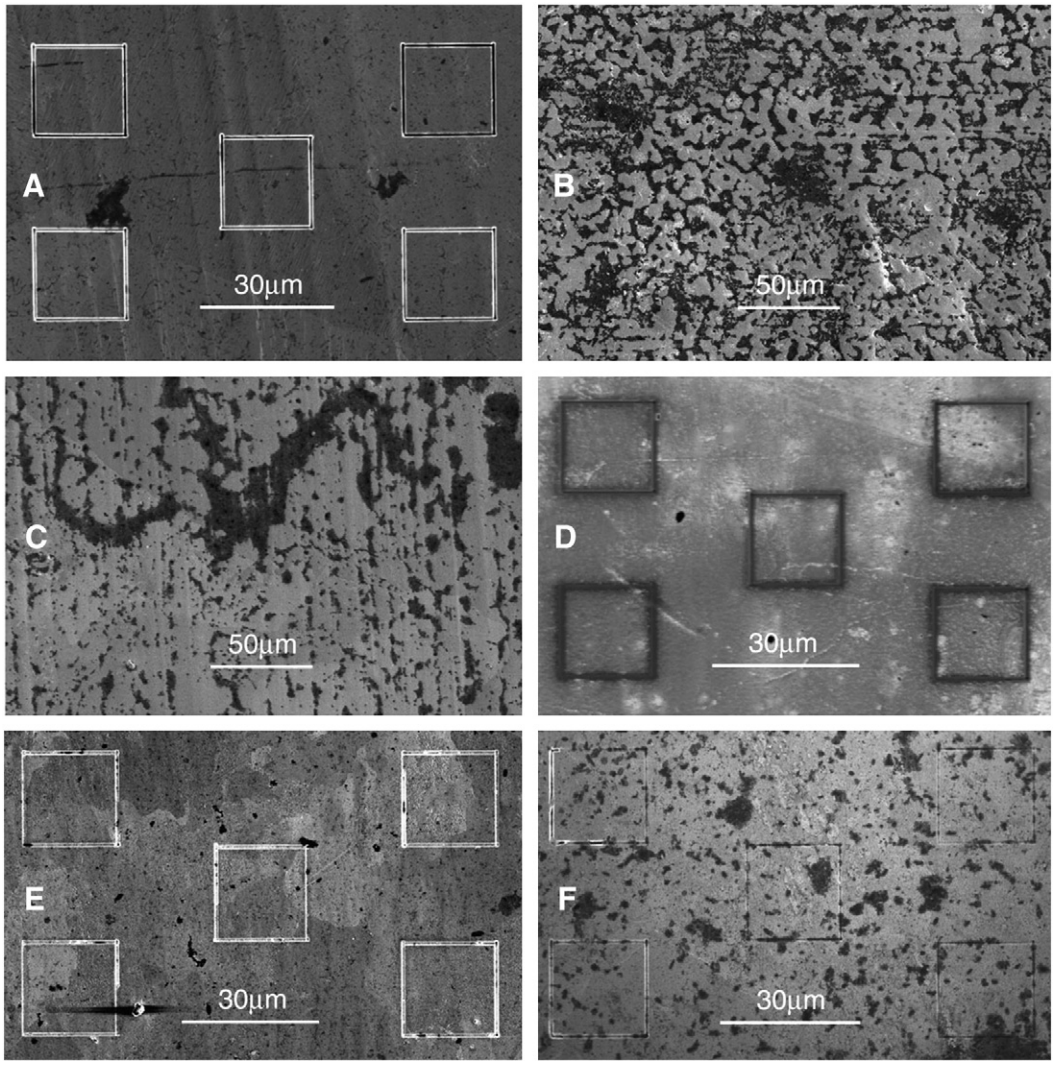

Fig. 7. SEM micrographs illustrating the results of experimental studies of the effect of biofilms on Au (A–C) and Pt (D–F) surfaces. (A), (B) and (C) represent the 56th day Au platelets incubated with growth medium, *C. violaceum* and *C. metallidurans*, respectively. (D), (E) and (F) represent the Pt platelets in the same order.

mobility, but there this is a much more episodic process (Fairbrother et al., 2012). Biofilm formation increases the ability of metallophilic bacteria, *e.g.*, *C. metallidurans*, to detoxify Au-complexes *via* the formation of nano-particulate metallic Au, and hence increases the metal-resistance of the biofilm community on the whole (Reith et al., 2007). Other members of the biofilm community contribute to increasing Au solubility, mobility and toxicity by releasing amino acids, cyanide, thiosulfate and other ligands, in order to limit the growth of competing organisms (Lengke and Southam, 2007; Reith et al., 2007; Fairbrother et al., 2009). This perpetual cycling of Au *via* solubilization and re-precipitation in the biofilms plays a fundamental role in promoting Au dispersion and transforming coarse primary Au into nano- and micro-particulate Au. Nano- and micro particulate Au is available for further physical dispersion, *e.g.*, by solution transport and ingestion by soil macro-organisms grazing on biofilms (Reith et al., 2010).

In contrast, the lower toxicity of Pt-complexes means that in order to drive a biogenic cycle similar to that of Au, the concentrations of dissolved Pt need to reach levels that are >10 times higher than those of Au. While mobility of naturally occurring Pt has been implied in soils at a number of subtropical and tropical sites (*e.g.*, Bowles et al., 1994; Cabral et al., 2011), toxic concentrations of Pt are unlikely to occur at Fifield, given that no Pt was detected in the groundwater. Platinum was also not detected in *aqua regia* digests of soils overlying the mineralized zone at Fifield; in contrast Au concentrations in these soils reached up to 40 ng g^{-1} dry weight soil, confirming Au mobility and Pt immobility at the site (Kaminski, pers. comm.). This is also supported by the results of earlier microcosm studies with soils from semi-arid and moderate sites in nearby Peak Hill and Tomakin (New South Wales, Australia). These studies have shown that microbial processes contribute significantly to the solubilization of Au, with up to 80 wt.% of total Au being solubilized within 20 to 45 days of incubation, after which Au was re-adsorbed predominantly to the organic soil fractions (Fig. 2; Reith and McPhail, 2006, 2007).

It is worth noting that Pt toxicity may be further reduced by the capacity of Pt-complexes to irreversibly sorb to soil mineral phases, as shown by Butt et al. (2001). In their experiments with ferruginous soils from Ora Banda, Mn-oxide-rich soils from Mt. Keith, organic matter-, Fe-, calcrete- and Mn-rich soils, Butt et al. (2001) showed that Pt(II)-thiosulfate complexes were irreversibly adsorbed to ferruginous minerals. In addition, the study showed that secondary Fe-minerals were more efficient in sorbing Pt complexes than organic matter.

In conclusion, toxicity levels of Pt complexes are not high enough to drive biofilm development on isoferroplatinum grain surfaces, which would act as a catalyst for further Pt mobilization. This indicates that the higher toxicity of Au-complexes compared to Pt-complexes, combined possibly with the tendency of Pt complexes to sorb irreversibly to ferruginous materials, can drive the building up of biofilms on Au grains, which then increases the rate of Au dispersion by mediating

dissolution and precipitation reactions (Reith et al., 2010). This suggests that while Au mobility in the Fifield system is geobiologically driven, Pt mobility is essentially driven by geochemical and physical processes.

5. Conclusions

This study shows that active biofilms developing on the surface of Au grains can provide the missing link in explaining the high Au mobility in many environments. The complex interactions of organisms in biofilms are responsible for solubilizing Au (*e.g.*, generation of organic acids, cyanide) and transforming coarse Au into (nano)-particulate Au that is more reactive and available for mechanical transport, *e.g.*, by organisms that graze on biofilms. In contrast, under most regolith conditions, the toxicity of Pt around isoferroplatinum grains is not sufficient to drive an analogous response, which explains the contrast in Au and Pt mobility. The secondary arborescent Pt–Pd nuggets from alluvial deposits at Córrego Bom Sucesso, Brazil, which have aggregated from groundwater within sediments may be one remarkable exception (Fleet et al., 2002; Cabral et al., 2008). The occurrence of these aggregates in sands with poor buffering capability (as opposed to the more common ultramafic regolith profiles) indicates the possibility of formation under relatively high or low pH, under which conditions Pt toxicity may play a role in establishing biofilms and promoting PGE mobility (Fig. 6).

Acknowledgments

We acknowledge the Australian Research Council (fellowships DP0878903 to J.B. and DP20106946 to F.R.); the CSIRO Emerging Science program; Julie Smith and the Analytical Services Unit, CSIRO Land and Water, Adelaide; R. Williams, L. Green, and A. Netting from Adelaide Microscopy for support with the microanalyses; and the Rimfire Ltd. Pty. team for field support. Part of this research was undertaken on the X-ray Fluorescence Microscopy beamline at the Australian Synchrotron, Melbourne, Australia. The paper benefited from reviews by J. Fein, O. Thalhammer, and an anonymous reviewer. This paper is dedicated to Peter Blias, who got us excited about tomography and passed away prematurely.

References

Abramoff, M.D., Magalhaes, P.J., Ram, S.J., 2004. Image processing with ImageJ. Biophotonics International 11, 36–42.
Anthony, E.Y., Williams, P.A., 1994. Thiosulfate complexing of platinum group elements. In: Alpers, C.N., Blowes, D.W. (Eds.), Environmental Geochemistry of Sulfide Oxidation. American Chemical Society, Washington, DC, pp. 551–560.
Arganda-Carreras, I., Sorzano, C.O.S., Marabini, R., Carazo, J.M., de Solorzano, C.O., Kybic, J., 2006. Consistent and elastic registration of histological sections using vector-spline regularization. Lecture Notes in Computer Science. Springer, Berlin/Heidelberg, pp. 85–95.
Barnes, S., Liu, W., 2012. Pt and Pd mobility in hydrothermal fluids: evidence from komatiites and from thermodynamic modelling. Ore Geology Reviews 44, 49–58.
Benedetti, M., Boulègue, J., 1991. Mechanism of gold transfer and deposition in a supergene environment. Geochimica et Cosmochimica Acta 55, 1539–1547.
Bethke, C.M., 2008. Geochemical and Biogeochemical Reaction Modeling, second edition Cambridge University Press, New York (564 pp.).
Bowles, J.F.W., Gize, A.P., Cowden, A., 1994. The mobility of the Pt-group elements in the soils of the Freetown Peninsula, Sierra Leone. The Canadian Mineralogist 32, 957–967.
Brugger, J., Etschmann, B., Pownceby, M., Liu, W.H., Grundler, P., Brewe, D., 2008. Oxidation state of europium in scheelite: tracking fluid–rock interaction in gold deposits. Chemical Geology 257, 26–33.
Brugger, J., Pring, A., Reith, F., Ryan, C., Etschmann, B., Liu, W.H., O'Neill, B., Ngothai, Y., 2010. Probing ore deposits formation: new insights and challenges from synchrotron and neutron studies. Radiation Physics and Chemistry 79, 151–161.
Butt, C.R.M., Williams, P.A., Gray, D.J., Roberston, I.D.M., Schorin, K.H., Churchward, H.M., McAndrew, J., Barnes, S.J., Tenhoeff, M.F.J., 2001. Geochemical Exploration for platinum group elements in weathered terrain. CRC LEME Open File Report 85. Bentley, Australia (218 pp.).
Cabral, A.R., Tupinamba, M., Lehmann, B., Kwitko-Ribeiro, R., Vymazalova, A., 2008. Arborescent palladiferous gold and empirical Au_2Pd and Au_3Pd in alluvium from southern Serra do Espinhaco, Brazil. Neues Jahrbuch fuer Mineralogie-Abhandlungen 184, 329–336.
Cabral, A.R., Radtke, M., Munnik, F., Lehmann, B., Reinholz, U., Riesemeier, H., Tupinambá, M., Kwitko-Ribeiro, R., 2011. Iodine in alluvial Pt-Pd nuggets: evidence for biogenic precious-metal fixation. Chemical Geology 281, 125–132.
Cabri, L.J., Harris, D.C., Weiser, T.W., 1996. Mineralogy and distribution of the platinum-group mineral (PGM) placer deposits of the world. Exploration and Mining Geology 5, 73–167.
Checa, S.K., Espariz, M., Audero, M.E., Botta, P.E., Spinelli, S.V., Soncini, F.C., 2007. Bacterial sensing of and resistance to gold salts. Molecular Microbiology 63, 1307–1318.
Cook, S.J., Fletcher, W.K., 1994. Platinum distribution in soil profiles of the Tulameen ultramafic complex, southern British-Columbia. Journal of Geochemical Exploration 51, 161–191.
Cousins, C.A., Kinloch, E.D., 1976. Some observations on textures and inclusions in alluvial platinoids. Economic Geology 71, 1377–1398.
Crawford, A.J., Meffre, S., Squire, R.J., Barron, L.M., Falloon, T.J., 2007. Middle and Late Ordovician magmatic evolution of the Macquarie Arc, Lachlan Orogen, New South Wales. Australian Journal of Earth Sciences 54, 181–214.
Denecke, M.A., Somogyi, A., Janssens, K., Simon, R., Dardenne, K., Noseck, U., 2007. Microanalysis (micro-XRF, micro-XANES, and micro-XRD) of a tertiary sediment using microfocused synchrotron radiation. Microscopy and Microanalysis 13, 165–172.
Ehrlich, H.L., 1998. Geomicrobiology: its significance for geology. Earth-Science Reviews 45, 45–60.
Etschmann, B.E., et al., 2010. Reduced As components in highly oxidized environments: evidence from full spectral XANES imaging using the Maia massively parallel detector. American Mineralogist 95, 884–887.
Fairbrother, L.G., Shapter, J., Brugger, J., Southam, G., Pring, A., Reith, F., 2009. Effect of the cyanide-producing bacterium *Chromobacterium violaceum* on ultraflat Au surfaces. Chemical Geology 265, 313–320.
Fairbrother, L., Brugger, J., Shapter, J., Laird, J., Southam, G., Reith, F., 2012. Supergene gold formation: biogenic secondary and nano-particulate gold from arid Australia. Chemical Geology 320–321, 17–31.
Fleet, M.E., de Almeida, C.M., Angeli, N., 2002. Botryoidal platinum, palladium and potarite from the Bom Sucesso stream, Minas Gerais, Brazil: compositional zoning and origin. The Canadian Mineralogist 40, 341–355.
Fletcher, W.K., Cook, S.J., Hall, G.E.M., Scagel, R.K., Dunn, C.E., 1995. Enrichment of platinum and associated elements in organic seepage soils of the Tulameen ultramafic complex, Southern British-Columbia. Journal of Geochemical Exploration 54, 39–47.
Gadd, G.M., 2010. Metals, minerals and microbes: geomicrobiology and bioremediation. Microbiology 156, 609–643.
Gammons, C.H., 1995. Experimental investigations of the hydrothermal geochemistry of platinum and palladium: IV. The stoichiometry of Pt(IV) and Pd(II) chloride complexes at 100 to 300 °C. Geochimica et Cosmochimica Acta 59, 1655–1667.
Gammons, C.H., Bloom, M.S., 1993. Experimental investigation of the hydrothermal geochemistry of platinum and palladium .2. The solubility of PtS and PdS in aqueous sulfide solutions to 300 °C. Geochimica et Cosmochimica Acta 57, 2451–2467.
Gray, D.J., Schorin, K.H., Butt, C.R.M., 1996. Mineral associations of platinum and palladium in lateritic regolith, Ora Banda Sill, Western Australia. Journal of Geochemical Exploration 57, 245–255.
Hall, M.D., Foran, G.J., Zhang, M., Beale, P.J., Hambley, T.W., 2003. XANES determination of the platinum oxidation state distribution in cancer cells treated with platinum(IV) anticancer agents. Journal of the American Chemical Society 125, 7524–7525.
Hancock, R.D., Finkelstein, N.P., Evers, A., 1977. Linear free-energy relation involving formation-constants of palladium(II) and platinum(II). Journal of Inorganic and Nuclear Chemistry 39, 1031–1034.
Hattori, K.H., Cameron, E.M., 2004. Using the high mobility of palladium in surface media in exploration for platinum group element deposits: evidence from the Lac des Iles Region, northwestern Ontario. Economic Geology and the Bulletin of the Society of Economic Geologists 99, 157–171.
Hough, R.M., Noble, R.R.P., Hitchen, G.J., Hart, R., Reddy, S.M., Saunders, M., Vaughan, D., Lowe, J., Gray, D.J., Anand, R.R., Butt, C.R.M., Verrall, M., 2008. Naturally occurring gold nanoparticles and nanoplates. Geology 36, 571–574.
Hough, R.M., Noble, R.R.P., Reich, M., 2011. Natural gold nanoparticles. Ore Geology Reviews 42, 55–61.
Inzelt, G., Horányi, G., 2006. The nickel group (nickel, palladium, platinum). In: Scholz, F., Pickett, C.J. (Eds.), Encyclopedia of Electrochemistry: Inorganic Chemistry v. 7a. Encyclopedia of Electrochemistry. Wiley-VCH, Weinheim, pp. 497–528.
Johan, Z., Ohnenstetter, M., Slansky, E., Barron, L.M., Suppel, D., 1989. Platinum mineralization in the Alaskan-type intrusive complexes near Fifield, New-South-Wales, Australia .1. Platinum-group minerals in clinopyroxenites of the Kelvin Grove prospect, Owendale intrusion. Mineralogy and Petrology 40, 289–309.
Kenney, J.P.L., Song, Z., Bunker, B.A., Fein, J.B., 2012. An experimental study of Au removal from solution by non-metabolizing bacterial cells and their exudates. Geochimica et Cosmochimica Acta 87, 51–60.
Kepner, R.L., Pratt, J.R., 1994. Use of fluorochromes for direct enumeration of total bacteria in environmental-samples — past and present. Microbiological Reviews 58, 603–615.
Lengke, M., Southam, G., 2006. Bioaccumulation of gold by sulfate-reducing bacteria cultured in the presence of gold(I)-thio sulfate complex. Geochimica et Cosmochimica Acta 70, 3646–3661.
Lengke, M.F., Southam, G., 2007. The deposition of elemental gold from gold(I)-thiosulfate complexes mediated by sulfate-reducing bacterial conditions. Economic Geology 102, 109–126.
Lengke, M.F., Fleet, M.E., Southam, G., 2006. Morphology of gold nanoparticles synthesized by filamentous cyanobacteria from gold(I)-thiosulfate and gold(III)-chloride complexes. Langmuir 22, 2780–2787.
Lintern, M.J., Butt, C.R.M., 1993. Pedogenic carbonate: an important sampling medium for gold exploration in semi-arid areas. Exploration Research News 7, 7–11.

Lintern, M.J., Hough, R.M., Ryan, C.G., Watling, J., Verrall, M., 2009. Ionic gold in calcrete revealed by LA–ICP–MS, SXRF and XANES. Geochimica et Cosmochimica Acta 73, 1666–1683.
Lombi, E., de Jonge, M.D., Donner, E., Ryan, C.G., Paterson, D., 2011. Trends in hard X-ray fluorescence mapping: environmental applications in the age of fast detectors. Analytical and Bioanalytical Chemistry 400, 1637–1644.
Martinez-Criado, G., Somogyi, A., Homs, A., Tucoulou, R., Susini, J., 2005. Micro-x-ray absorption near-edge structure imaging for detecting metallic Mn in GaN. Applied Physics Letters 87, 61913 (3 pages).
Mayhew, L.E., Webb, S.M., Templeton, A.S., 2011. Microscale imaging and identification of Fe speciation and distribution during fluid–mineral reactions under highly reducing conditions. Environmental Science and Technology 45, 4468–4474.
McCready, A.J., Parnell, J., Castro, L., 2003. Crystalline placer gold from the Rio Neuquen, Argentina: Implications for the gold budget in placer gold formation. Economic Geology and the Bulletin of the Society of Economic Geologists 98, 623–633.
Mergeay, M., Nies, D.H., Schlegel, H.G., Gerits, J., Charles, P., van Gijsegem, F., 1985. Alcaligenes eutrophus CH34 is a facultative chemolithotroph with plasmid-bound resistance to heavy metals. Journal of Bacteriology 162, 328–334.
Miles, A.A., Misra, S.S., 1938. The estimation of the bactericidal power of the blood. Journal of Hygiene 38, 732.
Nakajima, A., 2003. Accumulation of gold by microorganisms. World Journal of Microbiology and Biotechnology 19, 369–374.
Nies, D.H., 1999. Microbial heavy-metal resistance. Applied Microbiology and Biotechnology 51, 730–750.
Northcote, K.H., 1979. A Factual Key for the Recognition of Australian Soils, 4th edition Rellim Technical Publications, Adelaide (124 pp.).
Pan, P., Wood, S.A., 1994. Solubility of Pt and Pd sulfides and Au metal in aqueous bisulfide solutions .2. Results at 200 °C to 350 °C and saturated vapor pressure. Mineralium Deposita 29, 373–390.
Petts, A.E., Hill, S.M., Worrall, L., 2009. Termite species variations and their importance for termitaria biogeochemistry: towards a robust media approach for mineral exploration. Geochemistry: Exploration, Environment, Analysis 9, 257–266.
Rayment, G.E., Higginson, F.R., 1992. Australian Laboratory Handbook of Soil and Water Chemical Methods. Method C1a. Inkata Press, Melbourne.
Reith, F., McPhail, D.C., 2006. Effect of resident microbiota on the solubilization of gold in soils from the Tomakin Park Gold Mine, New South Wales, Australia. Geochimica et Cosmochimica Acta 70, 1421–1438.
Reith, F., McPhail, D.C., 2007. Microbial influences on solubilisation and mobility of gold and arsenic in regolith samples from two gold mines in semi-arid and tropical Australia. Geochimica et Cosmochimica Acta 71, 1183–1196.
Reith, F., Rogers, S.L., McPhail, D.C., Webb, D., 2006. Biomineralization of gold: biofilms on bacterioform gold. Science 313, 233–236.
Reith, F., Lenke, M.F., Falconner, D., Craw, D., Southam, G., 2007. Winogradski review — the geomicrobiology of gold. The ISME Journal 1, 567–584.
Reith, F., Etschmann, B., Grosse, C., Moors, H., Benotmane, M.A., Monsieurs, P., Grass, G., Doonan, C., Vogt, S., Lai, B., Martinez-Criado, G., George, G.N., Nies, D.H., Mergeay, M., Pring, A., Southam, G., Brugger, J., 2009. Mechanisms of gold biomineralization in the bacterium *Cupriavidus metallidurans*. Proceedings of the National Academy of Sciences of the United States of America 106, 17757–17762.
Reith, F., Fairbrother, L., Nolze, G., Wilhelmi, O., Clode, P., Gregg, A., Parsons, J.E., Wakelin, S., Pring, A., Hough, R., Southam, G., Brugger, J., 2010. Nanoparticle factories: biofilms hold the key to gold dispersion and nugget formation. Geology 38, 843–846.
Reith, F., Etschmann, B., Dart, R.C., Brewe, D.L., Vogt, S., Mumm, A.S., Brugger, J., 2011. Distribution and speciation of gold in biogenic and abiogenic calcium carbonates — implications for the formation of gold anomalous calcrete. Geochimica et Cosmochimica Acta 75, 1942–1956.
Reith, F., Brugger, J., Zammit, C., Gregg, A.L., Goldfarb, K., Andersen, G.L., DeSantis, T.Z., Piceno, Y.M., Brodie, E.L., Zhou, J., He, Z., Wakelin, S.A., 2012a. Influence of geogenic factors on microbial communities in metallogenic Australian soils. The ISME Journal 2012, 1–12.
Reith, F., Stewart, L., Wakelin, S.A., 2012b. Supergene gold transformation: secondary and nano-particulate gold from southern New Zealand. Chemical Geology 320, 32–45.
Ryan, C.G., 2000. Quantitative trace element imaging using PIXE and the nuclear microprobe. International Journal of Imaging Systems and Technology 11, 219–230.
Ryan, C.G., Etschmann, B.E., Vogt, S., Maser, J., Harland, C., van Achterbergh, E., Legnini, D., 2005. Nuclear microprobe — synchrotron synergy: towards integrated quantitative real-time elemental imaging using PIXE and SXRF. Proceedings of the ICNMTA'2004 conference. Nuclear Instruments and Methods in Physics 231, 183–188.
Ryan, C.G., et al., 2009. High-throughput X-ray fluorescence imaging using a massively parallel detector array, integrated scanning and real-time spectral deconvolution. In: David, C., Nolting, F., Quitmann, C., Stampanoni, M., Pfeiffer, F. (Eds.), 9th International Conference on X-Ray Microscopy. J. Phys. Con. Ser.
Ryan, C.G., Kirkham, R., Hough, R.M., Moorhead, G., Siddons, D.P., de Jonge, M.D., Paterson, D.J., De Geronimo, G., Howard, D.L., Cleverley, J.S., 2010a. Elemental X-ray Imaging Using the Maia Detector Array: The Benefits and Challenges of Large Solid-angle: Nucl. Instru. Meth.in Physics Research Section A — Accelerators Spectrometers Detectors and Associated Equipment, 619, pp. 37–43.
Ryan, C.G., Siddons, D.P., Kirkham, R., Dunn, P.A., Kuczewski, A., Moorhead, G., De Geronimo, G., Paterson, D.J., de Jonge, M.D., Hough, R.M., Lintern, M.J., Howard, D.L., Kappen, P., Cleverley, J., 2010b. The new Maia Detector System: methods for high definition trace element imaging of natural material. In: Denecke, M.A., Walker, C.T. (Eds.), X-Ray Optics and Microanalysis, Proceedings. AIP Conference Proceedings, pp. 9–17.
Sassani, D.C., Shock, E.L., 1998. Solubility and transport of platinum-group elements in supercritical fluids: summary and estimates of thermodynamic properties for ruthenium, rhodium, palladium, and platinum solids, aqueous ions, and complexes to 1000 ° C and 5 kbar. Geochimica et Cosmochimica Acta 62, 2643–2671.
Slansky, E., Johan, Z., Ohnenstetter, M., Barron, L.M., Suppel, D., 1991. Platinum mineralization in the Alaskan-type intrusive complexes near Fifield, NSW, Australia .2. Platinum-group minerals in placer deposits at Fifield. Mineralogy and Petrology 43, 161–180.
Song, Z., Kenney, J.P.L., Fein, J.B., Bunker, B.A., 2012. An X-ray fine structure study of Au absorbed onto the non-metabolizing cells of two soil bacteria species. Geochimica et Cosmochimica Acta 86, 103–117.
Southam, G., Saunders, J.A., 2005. The geomicrobiology of ore deposits. Economic Geology 100, 1067–1084.
Southam, G., Lengke, M.F., Fairbrother, L., Reith, F., 2009. The biogeochemistry of gold. Elements 5, 303–307.
Suárez, S., Prichard, H.M., Velasco, F., Fisher, P.C., McDonald, I., 2010. Alteration of platinum-group minerals and dispersion of platinum-group elements during progressive weathering of the Aguablanca Ni–Cu deposit, SW Spain. Mineralium Deposita 45, 331–350.
Usher, A., McPhail, D.C., Brugger, J., 2009. A spectrophotometric study of aqueous Au(III) halide-hydroxide complexes at 25–80 °C. Geochimica et Cosmochimica Acta 73, 3359–3380.
Watterson, J.R., 1992. Preliminary evidence for the involvement of budding bacteria in the origin of Alaskan placer gold. Geology 20, 315–318.
Watterson, J.R., 1994. Artifacts resembling budding bacteria produced in placer-gold amalgams by nitric-acid leaching. Geology 22, 1144–1146.
Wiesner, M.R., Lowry, G.V., Alvarez, P., Dionysiou, D., Biswas, P., 2006. Assessing the risks of manufactured nanomaterials. Environmental Science and Technology 40, 4336–4345.
Wood, S.A., 2002. In: Cabri, L.J. (Ed.), The Aqueous Geochemistry of the Platinum-group Metals with Applications to Ore Deposits. : The Geology, Geochemistry, Mineralogy and Mineral Beneficiation of Platinum-group Elements, Spec. vol. 6. Canadian Institute of Mining, Metallurgy and Petroleum, pp. 211–249.
Wood, S.A., Mountain, B.W., Pan, P., 1992. The aqueous geochemistry of platinum, palladium and gold—recent experimental constraints and a reevaluation of theoretical predictions. The Canadian Mineralogist 30, 955–982.